Improved dissipative particle dynamics simulations of lipid bilayers

Lianghui Gao, Julian Shillcock, and Reinhard Lipowsky[a)]
Max Planck Institute of Colloids and Interfaces, Potsdam 14424, Germany

(Received 17 August 2006; accepted 28 November 2006; published online 4 January 2007)

The authors introduce a new parameterization for the dissipative particle dynamics simulations of lipid bilayers. In this parameterization, the conservative pairwise forces between beads of the same type in two different hydrophobic chains are chosen to be less repulsive than the water-water interaction, but the intrachain bead interactions are the same as the water-water interaction. For a certain range of parameters, the new bilayer can only be stretched up to 30% before it ruptures. Membrane tension, density profiles, and the in-plane lipid diffusion coefficient of the new bilayer are discussed in detail. They find two kinds of finite size effects that influence the membrane tension: lateral finite size effects, for which larger membranes rupture at a smaller stretch, and transverse finite size effects, for which tensionless bilayers are more compact in larger systems. These finite size effects become rather small when the simulation box is sufficiently large. © *2007 American Institute of Physics*. [DOI: 10.1063/1.2424698]

I. INTRODUCTION

Lipid bilayer membranes play very important roles in the living cell.[1] Their structure and dynamic properties have attracted both experimental and theoretical interests.[2] Much progress has been made in measuring the bilayer elastic bending and area stretch moduli,[3] shape fluctuations,[4] and pore formation.[5] Dynamical processes, such as domain formation[6] and membrane fusion,[7] have also been investigated widely. In order to understand the dependence of the membrane's stability and material properties on its composition, and its component's molecular structure, various theoretical approaches have been developed, such as mean-field techniques,[8,9] Monte-Carlo simulation,[10] atomic molecular dynamics (MD) simulations,[11] and coarse grained (CG) MD simulations.[12–16]

Coarse grained simulations make it possible to study the assembly and properties of amphiphilic membranes on relatively large temporal and spatial length scales. CG simulation techniques reach large length scales by combining molecule groups into particles or beads, and long time scales by replacing atomistic forces with soft effective forces. Dissipative particle dynamics (DPD) simulation[17–19] is one CG technique that has been recently used to study soft materials, such as the self-assembly of amphiphilic micelle and bilayers.[20–24] In the DPD method, the thermostat is provided by dissipative and random forces, which act together with short-ranged conservative forces. The equilibrium structure and elastic properties of fluid bilayer membrane patches simulated by DPD are in good agreement with experimental results. DPD simulations have also been applied successfully in the investigation of the dynamic process of membrane fusion.[25]

As a result of coarse graining, the force parameters explicitly used in the DPD model are not directly related to molecular-scale interactions. Consequently, the material properties are only accurate over a certain parameter range. For example, the lipid bilayer simulated by DPD exhibits a reasonable equilibrium structure near the tensionless state, but it is too stretchable to be ruptured easily.[21] In these DPD simulations, the bilayer ruptures after its area is stretched by 60%,[21] but large lipid vesicles can only resist 5% strain.[26,27] In this article, we introduce a new parameterization for a less stretchable bilayer and describe two types of finite size effects on the bilayer's compressibility. The latter quantity is crucial for understanding many dynamic processes occurring in the membrane, such as membrane fusion and cell lysis induced by antimicrobial peptides.

In all previous DPD models of lipid bilayers, the values of the conservative repulsive force parameters between two amphiphilic beads (head beads or tail bead) of the same type are set equal to water-water interaction.[20–24] Such simple modeling ensures that the lipids can self-associate to well ordered fluid bilayer. But it ignores the detailed molecular interactions, such as van der Waals forces, which should lead to effective interactions that are different for water-water bead pairs and amphiphile-amphiphile bead pairs. One consequence of the simplified modeling is that the bilayer obtained in this way is rather stretchable and a large degree of strain is required to produce a pore in the bilayer. In this article, we modify the force parameters of DPD to simulate lipid bilayer in water. Here we set the forces between the same kind of lipid beads in different chains to be less repulsive than the water-water interaction. At the same time, we keep the force between two beads belonging to the same chain to be identical to the water-water interaction, which guarantees that the amphiphilic beads have the same coarse grained size as the water beads. The inclusion of less repulsive interchain forces makes the bilayer less stretchable. For a certain range of parameters, the area of the bilayer obtained by this new model can only be stretched up to 30% before it ruptures. The membrane thickness and bending rigidity of this new bilayer are consistent with real dimyristoylphos-

[a)]Electronic mail: lipowsky@mpikg.mpg.de

phatidylcholine (DMPC) bilayer. We also find lateral and transverse finite size effects that influence the membrane tension and membrane thickness, which have not been discussed before. The new parameter set will be used in a separate publication in order to explore the membrane fusion of two vesicles.

The article is organized as follows. In Sec. II, we give a brief introduction of the DPD method to simulate amphiphilic molecules in water. Then we optimize the force parameters to simulate less stretchable lipid bilayers in Sec. III. The properties of the new lipid bilayers, such as membrane tension, density profile, area compressibility, and diffusion coefficients are discussed in detail in Sec. IV. In Sec. V, we discuss the finite size effects and volume compressibility. Our final conclusions are given in Sec. VI.

II. METHOD OF DISSIPATIVE PARTICLE DYNAMIC SIMULATIONS

DPD was introduced to simulate the hydrodynamic behavior of fluids. The elementary units of DPD simulations are soft beads with mass m_0 and diameter r_0, whose dynamics are governed by Newton's law supplemented by friction and random forces that provide the thermostat of the system.[17–19] Each bead represents the fluid volume of several molecules. Two beads at position $\mathbf{r}_i$ and $\mathbf{r}_j$ with separation vector $\mathbf{r}_{ij} \equiv \mathbf{r}_i - \mathbf{r}_j$ and unit vector $\hat{\mathbf{r}}_{ij} \equiv \mathbf{r}_{ij}/|\mathbf{r}_{ij}|$ experience three types of forces: the conservative force,

$$F_{ij}^C = a_{ij}(1 - r_{ij}/r_0)\hat{r}_{ij}, \tag{1}$$

the random force,

$$F_{ij}^R = \sqrt{2\gamma_{ij}k_BT}(1 - r_{ij}/r_0)\zeta_{ij}\hat{r}_{ij}, \tag{2}$$

and the dissipative force,

$$F_{ij}^D = -\gamma_{ij}(1 - r_{ij}/r_0)^2(\hat{r}_{ij} \cdot \mathbf{v}_{ij})\hat{r}_{ij}, \tag{3}$$

for $r_{ij} < r_0$. Here the vectors $\mathbf{v}_{ij} \equiv \mathbf{v}_i - \mathbf{v}_j$ are the velocity differences between particle i and j. The parameters a_{ij} represent the repulsion strengths, γ_{ij} are the friction coefficients, and the random numbers ζ_{ij} are symmetrically and uniformly distributed with $\langle \zeta_{ij}(t) \rangle = 0$ and $\langle \zeta_{ij}(t)\zeta_{i'j'}(t') \rangle = (\delta_{ii'}\delta_{jj'} + \delta_{ij'}\delta_{ji'})\delta(t-t')$. The factor k_BT represents the thermal energy at temperature T and ensures that the equilibrium system satisfies the fluctuation-dissipation theorem. The DPD simulations described here are performed in the *NVT* ensemble. The soft core potential and DPD thermostat both permit larger time steps than in coarse grained molecular dynamics simulations. Note that DPD is not limited to soft core interactions, but can also be applied to "hard" particles that interact via Lennard-Jones potentials.[28]

One should note that the parameterization of the random forces ζ_{ij} as described in the previous paragraph corresponds to continuous time. These forces have the physical dimension of 1 over square root of time. In the numerical simulations, the equations of motion are discretized in time using a small time step Δt. In order to ensure that the diffusion coefficient of the particles or beads is independent of the choice for Δt, one uses the change of variables as given by $\zeta_{ij} \equiv \zeta'_{ij}/\sqrt{\Delta t}$ where the rescaled random force ζ'_{ij} is dimensionless and has a variance that does not depend on Δt; a more detailed discussion of this point is given in Ref. 19.

TABLE I. Conservative force parameter a'_{ij} (in unit of k_BT/r_0) used in the previous paper (Ref. 21).

a'_{ij}	H	C	W
H	25	50	35
G	50	25	75
W	35	75	25

To simulate amphiphilic lipids in aqueous solution, the solvent is modeled as a single bead (denoted by W) with diameter r_0 and mass m_0. It is assumed that each water bead represents three water molecules. The lipid molecules are mapped to 11 bead polymers with the same molecular architecture as in Ref. 12. This polymer has three hydrophilic head beads (denoted by H) connected in a chain via harmonic springs with potential

$$U_2(i, i+1) = \tfrac{1}{2}k_2(r_{i,i+1} - l_0)^2. \tag{4}$$

Two hydrophobic chains, each of which is composed of four hydrocarbon beads (denoted by C), are attached to two adjacent head beads (see Fig. 3 in Ref. 12). In order to model the chain stiffness, three adjacent chain beads experience the three-body potential,

$$U_3 = k_3[1 - \cos(\phi)], \tag{5}$$

where ϕ is the angle between the two bonds connecting beads $i-1$, i, and $i+1$. The head and tail beads are all assumed to have the same mass and density as water beads.

III. FORCE PARAMETER OPTIMIZATION

The set of previously used conservative force parameters a'_{ij} in Eq. (1) is listed in Table I. All the other parameters that enter in Eqs. (1)–(5) are identical to those used in Ref. 21: the friction parameters γ_{ij}, which enter the dissipative force as given by Eq. (3), have the numerical values $\gamma_{HH} = \gamma_{CC} = \gamma_{WW} = \gamma_{HW} = 4.5\sqrt{k_BTm_0/r_0^2}$, $\gamma_{HC} = 9\sqrt{k_BTm_0/r_0^2}$, $\gamma_{CW} = 20\sqrt{k_BTm_0/r_0^2}$, the spring constant k_2 in Eq. (4) is given by $k_2 = 128k_BT/r_0^2$, the spring length l_0 in Eq. (4) has the value $l_0 = 0.5r_0$, and the bending stiffness k_3 in Eq. (5), is taken to be $k_3 = 20k_BT$. In the simulations, all length scales are measured in units of the bead diameter r_0 and all forces in units of k_BT/r_0. Likewise, all time scales are given in units of $t_0 \equiv \sqrt{m_0r_0^2/k_BT}$ where m_0 is the bead mass. For a certain range of surfactant number fractions (or concentration), the amphiphiles aggregate into well-ordered bilayer structures because of the strong repulsion a_{CW} between the chain beads and the solvent beads, mimicking the hydrophobic effect for hydrocarbon chains in water.[21] Kranenburg *et al.*[24] studied the formation of lipid bilayers by using various parameter sets. They found that a bilayer can always be obtained as long as the phospholipid has well-defined hydrophilic and hydrophobic parts. In all of those previously used parameter sets, the interactions between the same kind of lipid beads, a_{HH} and a_{CC}, are chosen to be the same as the water-water beads interaction a_{WW}. This choice ensures that the head and

TABLE II. Conservative force parameter a_{ij} (in unit of k_BT/r_0) introduced in this article.

a_{ij}	H	C	C_e	W
H	25 (20)[a]	30	30	25
C	30	25 (10)[a]	25 (15)[a]	60
C_e	30	25 (15)[a]	15	60
W	25	60	60	25

[a]The value outside the bracket is the intrachain strength; the value inside the bracket is the interchain strength.

tail beads have the same mass, volume, and density as water beads. But the high stretchability of the bilayer corresponding to the parameters a'_{ij} in Table I (Ref. 21) implies that the bilayer is rather soft and difficult to rupture. To simulate less stretchable bilayers, we need to modify the force parameters. The new values denoted by a_{ij} are listed in Table II. We will discuss in detail why we chose these parameters in the following. All the other parameters are kept the same as in Ref. 21.

It is plausible that one can decrease the stretchability of the bilayer membrane by making the interactions between the lipid molecules more attractive and/or less repulsive. Indeed, by lowering the repulsive strength a_{CC} between all tail beads, we found a dramatic reduction of the stretchability. But we observe an unexpected side effect: The length of the lipid tails becomes shorter and the membrane becomes thinner, which indicates that the 11-bead model cannot represent the real lipid molecule any more. There are several ways in which one can address this problem: one can (i) increase the equilibrium bond length l_0, (ii) add one or more tail beads to the hydrophobic chain, or (iii) modify the interchain and intrachain force parameter a_{CC}. In this article, we treat the interchain and intrachain interaction parameter a_{CC} differently. For the tail beads along the same chain (intrachain), the parameter a_{CC} is set equal to $a_{WW}=25$. For the tail beads not in the same chain (interchain), the parameter a_{CC} is set to be 10 which is less repulsive than a_{WW}. This choice enables us to obtain less stretchable bilayers with a coarse grained polymer length that is comparable to that of real lipid molecules. One thing we noticed here is that once $a_{CC}<a_{WW}$, the bilayer is in the interdigitation phase rather than in the fluid phase which can be seen from the density profile of the tail beads that has a sharp peak in the center (data not shown). This is because the interchain tail-tail bead repulsion $a_{CC} \neq a_{WW}$ allows the tails to penetrate and thus occupy less volume than water beads. To obtain a bilayer without interdigitation in the new DPD model, we should allow the end-chain tail beads (denoted by C_e) to occupy more volume (or to be more flexible). Thus, if one or both of the tail beads are at the end of the hydrophobic chain, the tail-tail bead interaction is taken to be $a_{C_eC_e}=a_{CC_e}=15>a_{CC}=10$.

The head-head repulsive parameter a_{HH} modulates the bilayer's spontaneous curvature and bending rigidity: larger values of a_{HH} tend to introduce positive curvature and to lower the bending rigidity, while smaller values of a_{HH} cause negative curvature and increase the bending rigidity. In our model with interchain parameter $a_{CC}=10$, we find that the lipids can self-assemble to well-ordered bilayers if the interlipid force strength a_{HH} is in the range of 15–25. In order to obtain a less stretchable bilayer with a bending rigidity comparable to experimental values, we choose $a_{HH}=20$. In order to obtain a realistic ratio between molecular area and bilayer thickness, we again choose the intralipid head-head parameter a_{HH} to be equal to the water-water interaction $a_{WW}=25$.

In principle the parameters a_{ij} for $i \neq j$ can be obtained from the corresponding Flory-Huggins χ parameter.[19,20] But a complete set of experimental χ values for lipids in water are not available. So in DPD simulations, trails of a_{ij} have to be made to obtain bilayer whose structure and dynamic properties are in good agreement with real lipid bilayers. In the following discussion, we will explain how we chose these parameters.

The parameter a_{HW} represents the force between lipid head groups and water beads. For relatively large values of a_{HW}, the head beads are not sufficiently excluded from the hydrophobic core, and the bilayer is not stable. Therefore, smaller values of a_{HW} can successfully keep the water outside the hydrophobic core. We also find, however, that the bilayers exhibit strong undulations for small a_{HW}, and two vesicles cannot adhere, irrespective of the initial separation. This is because the attraction between the two membranes cannot overcome the strong hydration force and, thus, cannot repel the water out of the contact region effectively. We find that $a_{HW}=25$ represents the best choice in order to get well-ordered bilayers which can adhere to each other.

The interaction parameter a_{HC} determines the flip-flop rate of the lipids. Large values of a_{HC} stabilize the bilayer but lower the flip-flop rate. In the dynamics of membrane fusion, a_{HC} determines whether the lipids in the two outmost leaflets can easily mix or not. Because we aim to use the new parameter set to study the fusion of two vesicles, we have chosen $a_{HC}=30$ as this leads to a reasonable rate of lipid mixing at sufficiently large membrane tension.

The interaction parameter a_{CW} represents the hydrophobic force between tail beads and water beads. Lipid molecules form well-ordered bilayer structures for large values of a_{CW}. Here we choose $a_{CW}=60$. This value combined with $a_{HW}=25$ and $a_{HC}=30$ leads to a bilayer with the desired structure and elastic properties.

IV. PROPERTIES OF THE NEW BILAYER

In this section, we discuss the properties of the planar bilayer simulated by using the new parameter set in Table II, such as the stretchability, area compressibility, bending rigidity, and diffusion coefficient.

First we simulate $N=1480$ lipids in a box with fixed volume $V=L_\parallel^2 L_\perp=32\,768r_0^3$. The total density of the system is $\rho=3/r_0^3$ which corresponds to the total bead number $N_t=3V/r_0^3=98\,304$ in the system. Note that $N_t=N_w+11N$ since each lipid molecule consists of 11 beads. The time step used here is $\Delta t=0.02t_0$ with the characteristic time scale $t_0=\sqrt{m_0r_0^2/k_BT}$ that will be related to real time in the last paragraph of this section. A typical run of 10^5 time steps for such a system takes 72 h on an Intel XEON processor (CPU 3.06 GHz). To save computing time, the lipid molecules are initially arranged in a planar bilayer state consisting of two

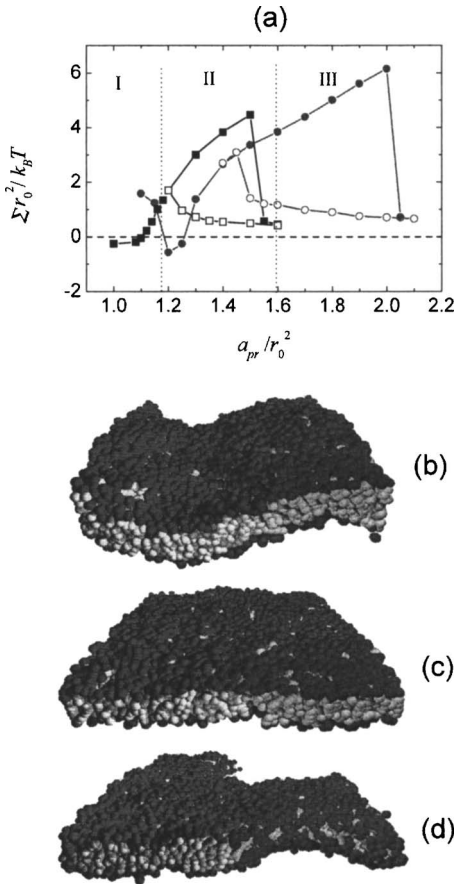

FIG. 1. (a) Surface tension Σ vs projected area per lipid molecule for 1480 lipids in a simulation box with fixed volume $V=32\,768r_0^3$. The filled squares correspond to the new parameters in Table II, the filled circles to the old parameters in Table I. The open squares and circles are results for bilayers initially containing a small circular pore. The bilayers with the new parameterization exhibit the three regimes I, II, and III as the projected area is increased. Typical bilayer conformations in these three regimes are shown in (b), (c), and (d) respectively. In these snapshots, lipid head beads are red, tail beads are yellow, and water beads are invisible.

adjacent monolayers with their hydrophilic heads pointing towards the water. We also checked, however, that randomly distributed lipids do self-assemble to such a planar bilayer for a small box with size $(16\times16\times16)r_0^3$. As mentioned previously, the units for length, time, and energy are taken to be r_0, $\sqrt{m_0r_0^2/k_BT}$, and k_BT, respectively, for all simulation data.

The rupture behavior of the bilayer under tension is shown in Fig. 1(a), where we calculate the membrane tension Σ as a function of the projected area per lipid a_{pr}. The parameter $a_{\mathrm{pr}}=2L_{\parallel}^2/N$ is varied by modifying the lateral size $L_{\parallel}$ while keeping the number of lipid molecules and system volume fixed. (The calculation of the surface tension is performed as in Ref. 12) To obtain the values of membrane tension, the first 50 000 time steps are discarded to exclude the influence of the initial state. Subsequently, we average 1000 independent configurations. The configurations are taken every 50 time steps, which is longer than the typical correlation time as estimated from the potential correlation function. There are three regimes in Fig. 1(a). In regime I, the intrinsic area of the bilayer is larger than the projected area. The bilayer has negative surface tension and tends to form multilamellar phase. One snapshot corresponding to this regime is shown in Fig. 1(b). The bilayer is relaxed (or tensionless) for projected area $a_0\simeq1.12r_0^2$ and becomes tense at larger projected area, as shown in Fig. 1(a) as regime II. For $a_{\mathrm{pr}}>a_0$, the intrinsic area is essentially equal to the projected area. The bilayer is rather flat and hardly fluctuates as displayed in Fig. 1(c). The largest tension that the bilayer can sustain is $4.6k_BT/r_0$ at $a_{\mathrm{pr}}^{\mathrm{rup}}=1.5r_0^2$. Close to this critical area, we run six independent simulations for each value of the projected area. The rupture area $a_{\mathrm{pr}}^{\mathrm{rup}}=1.5r_0^2$ is taken to be the smallest area for which no rupture is observed within the simulation time. The bilayer ruptures by opening a pore as in Fig. 1(d). The decrease of surface tension starting at area $a_{\mathrm{pr}}=1.55r_0^2$ indicates the pore opening. So the stretchability of the bilayer is $(a_{\mathrm{pr}}^{\mathrm{rup}}-a_0)/a_0\simeq35\%$, which should be compared to the corresponding value of 60% for the old parameters in Table I.[21] The stretchability becomes even smaller if we increase the system size as explained in the next section. For large vesicles, due to the curvature, the stretchability can also be reduced by additional 5%–10% in our DPD simulations.

In order to explore the hysteresis of rupture, we also performed simulations for porated bilayers. The initial state was provided by a ruptured bilayer with a circular pore of radius $r_{\mathrm{po}}=3r_0$ in the center of the membrane patch. To create such a pore, we first assemble a nonruptured bilayer with $N+N\zeta$ lipid molecules with projected area $L_{\parallel}^2=Na_{\mathrm{pr}}/2$. We then define a circular pore with radius r_{po} via $\pi r_{\mathrm{po}}^2=L_{\parallel}^2\zeta=N\zeta a_{\mathrm{pr}}/2$. After 5000 time steps which ensure that there is no initial defect in the bilayer, we replace the $N\zeta$ lipids inside a cylindrical shell with radius r_{po} at the center of the membrane by $11N\zeta$ water beads. The pore reseals quickly if the projected area per lipid a_{pr} is less than $1.25r_0^2$. The corresponding resealing tension of such a porated bilayer is 12 mN/m which is in the range of experimental value.[29] For $a_{\mathrm{pr}}\geqslant1.25r_0^2$, the pore grows to its equilibrium size. The open squares in Fig. 1(a) are the membrane tensions simulated from such initial conditions. We see that the membrane tension values are reduced compared to simulations starting with initially nonruptured bilayer with $a_{\mathrm{pr}}\geqslant1.25r_0^2$. As the projected area is further decreased, the open squares start to coincide with bilayers without an initial pore. In Fig. 1(a), the filled squares, which correspond to an unporated bilayer under increasing tension, and the open squares, which represent a porated bilayer under decreasing tension, provide an estimate for the hysteresis loop associated with rupture. If the unporated bilayer is stretched up to a projected molecular area that exceeds $a_{\mathrm{pr}}=1.5r_0^2$, it will rupture within about 4 μs; if the porated bilayer has a projected molecular area of less than $a_{\mathrm{pr}}=1.25r_0^2$, it will reseal within about 4 μs. As we increase the projected molecular area a_{pr} of the unporated bilayer to values above $a_{\mathrm{pr}}=1.5r_0^2$, the average rupture time should decrease monotonically. For a sufficiently large value $a_{\mathrm{pr}}=a_>$, the average rupture time should attain a limiting value that reflects the minimal time necessary to create a water channel across the bilayer. Likewise, if we decrease the projected molecular area of the porated bilayer to values below $a_{\mathrm{pr}}=1.25r_0^2$, the average resealing time should also decrease monotonically. For a sufficiently small $a_{\mathrm{pr}}=a_<$, the

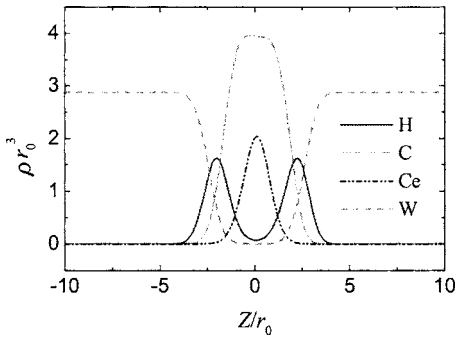

FIG. 2. Density profiles of a bilayer with 1480 lipids and projected molecule area $a_{pr}=1.14r_0^2$ as a function of the coordinate Z perpendicular to the bilayer. The four profiles corresponds to head groups (H), tail beads (C), end-chain tail beads (C_e), and water beads (W).

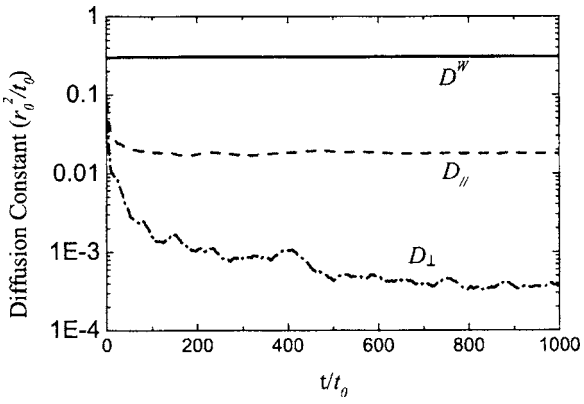

FIG. 3. Effective diffusion constants for water beads and lipid molecules as a function of time t. Data are obtained for a system with 1480 lipids, volume $V=32\,768r_0^3$, and projected area per lipid molecule $a_{pr}=1.14r_0^2$. The full, dashed, and dot-dashed lines represent the effective diffusion constants for water beads, lateral diffusion of lipids, and transverse diffusion of lipids, respectively.

average resealing time will attain a limiting value that reflects the minimal time needed to push the water out of the pore. In order to determine the precise values of $a_<$ and $a_>$, one would have to perform a large number of simulation runs from which one can extract the distribution for the resealing and rupture times. Such a computationally demanding study remains to be done.

The density profiles of head, tail, and water beads of a tensionless bilayer with 1480 lipids are shown in Fig. 2. The narrow distribution of head beads shows that the lipids are in a bilayer state. The smooth and flat tail bead distribution indicates that the bilayer is fluid and that the terminal tail beads are not interdigitating. Compared to the profiles simulated by the old parameters in Ref. 21, the main difference observed is the density profile of the hydrocarbon tail beads: due to the less repulsive strength between tail beads in different chains, the hydrophobic core is more compressed than the aqueous solution. From Figs. 1 and 2 we can derive the elastic properties of the bilayer: If we set a_0 equal to the measured value of 0.65 nm^2 for DMPC bilayers, we obtain $r_0 \simeq 0.76$ nm. The membrane thickness l_{me} is estimated to be 3.2 nm, in agreement with experimental values. We also measured the area compressibility K_A of the bilayer close to the zero tension state via $\Sigma=K_A(a_{pr}-a_0)/a_0$ (Ref. 13), and obtained the value $K_A=160$ dyn/cm^2. The bending rigidity κ is calculated via $\kappa=K_A l_{me}^2/48$,[13] which is about $8k_BT$.

To estimate the time scale in physical units, we also determined the lateral and transverse diffusion constants $D_{\|}$ and $D_\perp$ for the lipids and the total diffusion constant D^W for the water beads. For details of this calculation, the reader is referred to Ref. 12. For long time t, the diffusion constants attain constant values as shown in Fig. 3. Identifying the lateral diffusion constant of the lipid molecule as given by $D_{\|}=0.017r_0^2/t_0$ with a typical experimental value 5 μm^2/s, we obtain t_0 close to 2.0 ns, and the time step of $0.02t_0$ then corresponds to 0.04 ns.

V. FINITE SIZE EFFECTS

In general, one would like to understand the behavior of real systems from the behavior observed in the simulations. One obvious difficulty is that the system sizes accessible to simulations are rather small. In order to draw conclusions about the behavior of real systems, which are typically much larger, one needs to know how the system properties vary with the system size.

In the following, we will address two finite size effects that we have observed with respect to the membrane tension: (I) lateral finite size effects for fixed height $L_\perp$ of the simulation box and (II) transverse finite size effects for fixed lateral size $L_{\|}$ of this box.

A. Lateral finite size effects

Lateral finite size effects are observed by increasing (or decreasing) the lateral size $L_{\|}$ of the membrane patches as well as the volume of the simulation box by the same factor while keeping the total bead density ρ equal to 3. In Fig. 4(a), we plot the membrane tension as a function of projected area per lipid of three membrane patches with 740, 1480, and 2960 lipids in boxes with size $V_1=16\,384r_0^3$, $V_2=2V_1$, and $V_3=4V_1$, respectively. The lipid concentration is the same in all these systems. Moreover, for fixed $L_\perp$, the perpendicular pressure for the three systems is constant because the water layers have the same thicknesses. For each system size, we performed six runs and determined the projected molecular area of rupture a_{pr}^{rup} for each of these runs. The corresponding average value $\langle a_{pr}^{rup}\rangle$ was found to be $\langle a_{pr}^{rup}\rangle=(1.68\pm0.03)r_0^2$, $(1.58\pm0.04)r_0^2$, and $(1.58\pm0.05)r_0^2$ for volume $V=V_1$, V_2, and V_3, respectively. Thus, we did not observe a measurable decrease of $\langle a_{pr}^{rup}\rangle$ as we increased the system size from V_2 to $V_3=2V_2$. To determine the transition point between porated and unporated bilayers, we also run six independent simulations of the porated bilayers. For the small system with 740 lipids and volume V_1, we find that the six pores reseal unanimously at projected molecular area $a_{pr}^{res}=1.3r_0^2$. For the larger system with 1480 lipids and volume V_2, all of the six pores reseal at projected molecular area $a_{pr}^{res}=1.25r_0^2$. The resealing behavior shows similar lateral finite size effects to the rupture behavior. But the area difference between them does not strongly depend on the lateral size. Lateral finite size effects have also been observed in the coarse grained MD simulation performed in Ref. 30. The authors of this latter study

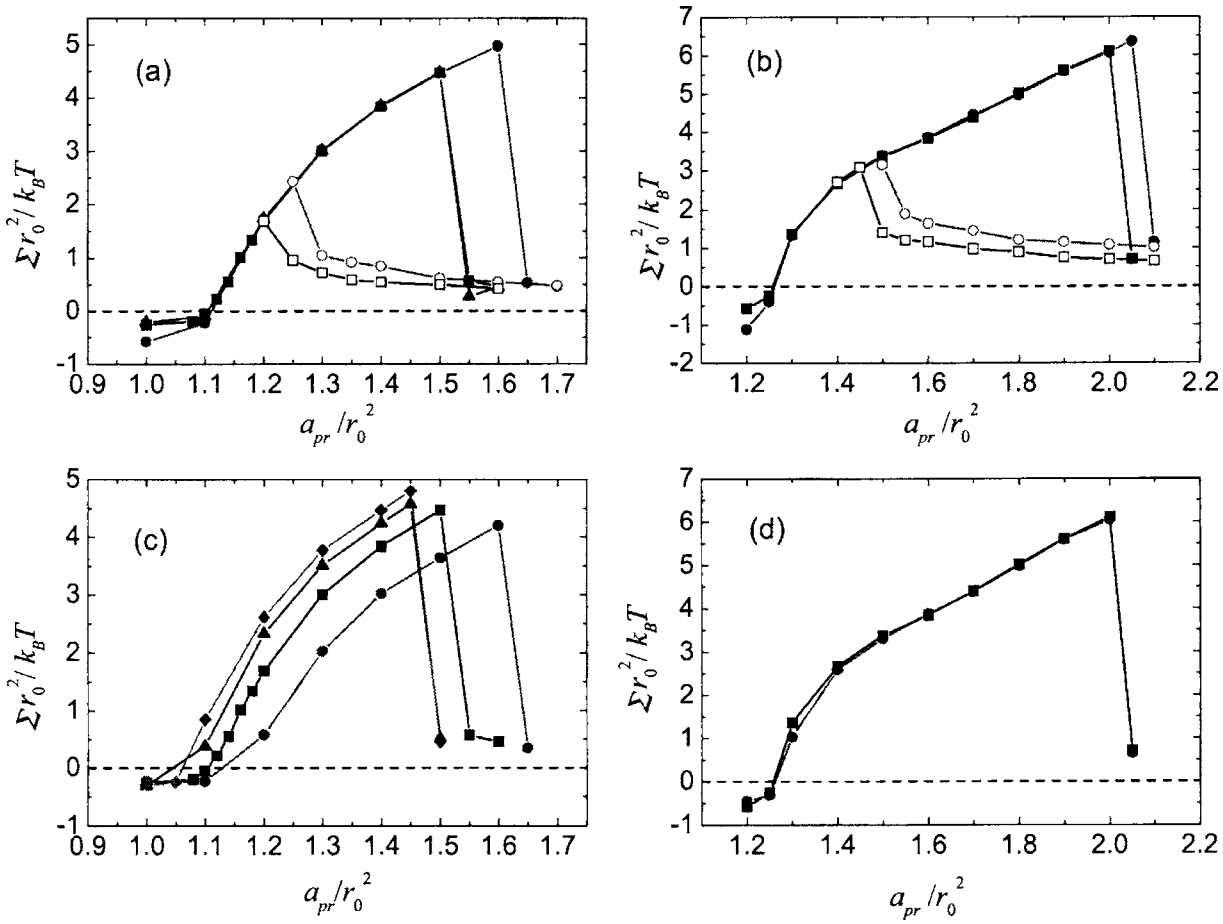

FIG. 4. Rescaled membrane tension Σ as a function of the rescaled projected area per lipid a_{pr}: (a) Lateral finite size effects obtained by using the new parameter set in Table II for 740 lipids in a simulation box with volume $V_1=16\,384r_0^3$ (circles), 1480 lipids in a box with volume $V_2=2V_1$ (squares), and 2960 lipids in a box with volume $V_3=4V_1$ (triangles). (b) Lateral finite size effects obtained by using the old parameter set in Table I for 740 lipid and volume $V_1=16\,384r_0^3$ (circles), 1480 lipids and volume $V_2=2V_1$ (squares). In (a) and (b), open and filled symbols correspond to bilayers initially with and without pores, respectively. (c) Transverse finite size effects obtained by using the new parameter set in Table II for 1480 lipids in simulation boxes with volume $V_1=16\,384r_0^3$ (circles), $V_2=2V_1$ (squares), $V_3=4V_1$ (triangles), and $V_4=8V_1$ (diamonds). (d) Absence of transverse finite size effects for the old parameter set in Table I and 1480 lipids in simulation boxes with volume $V_1=16\,384r_0^3$ (circles) and $V_2=2V_1$ (squares).

concluded that the stretchability of the bilayer membrane patch decays as an inverse power of the membrane area. Our simulations do not provide any clear evidence for this conclusion. In the previous DPD model with force parameters as given in Table I,[21] similar finite size effects have been observed as displayed in Fig. 4(b).

B. Transverse finite size effects

Next, we discuss transverse finite size effects that are characteristic for the *NVT* ensemble considered here. These latter effects arise as we increase the height and volume of the simulation box while keeping the lateral size of the membrane patch fixed. Furthermore, as in the case of the lateral finite size effects considered in the previous subsection, the total density of the system is also kept constant and equal to $\rho=3/r_0^3$. The latter constraint for the density ensures that the total density approaches the value of the water density in the limit of large box height. It also implies, however, that the water density and the perpendicular water pressure as observed in the simulations increase with the system volume as explained in the following.

In Fig. 4(c), we display the results for 1480 lipids in four boxes with volume $V_1=16\,384r_0^3$, $V_2=2V_1$, $V_3=4V_1$, and $V_4=8V_1$. We find that the tensionless state shifts to smaller projected area and that the bilayer ruptures at smaller strain with increasing system size. In the larger box, the water layers above and below the membrane patch are denser and thus exert more perpendicular pressure on the membrane, thereby making it thinner and less stretchable.

The total density ρ and the number N_W of water beads are related by $N_W=\rho V-11N$ where N denotes the number of lipid molecules as before. We now define the water volume via $V_W\equiv V-Nv_{\mathrm{mol}}$ where v_{mol} represents the volume of one lipid molecule. The water density ρ_W is then given by

$$\rho_W=\frac{N_W}{V_W}=\frac{\rho-11N/V}{1-v_{\mathrm{mol}}N/V}\approx\rho-(11-\rho v_{\mathrm{mol}})N/V, \qquad (6)$$

where the asymptotic equality applies to the limit of large volume V. Since the number N of lipid molecules is kept constant here, the water density ρ_W must become equal to the total density ρ for large V. Relation (6) implies that the leading correction term is of order $1/V$. The sign of this correction term depends on the numerical value for the molecular

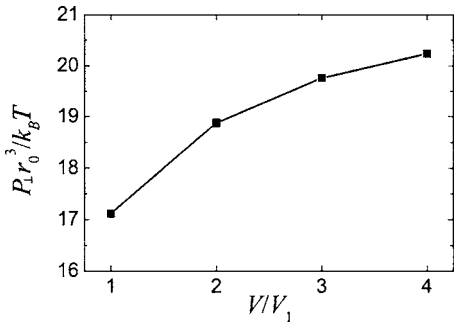

FIG. 5. Perpendicular water pressure $P_\perp$ exerted on the bilayer as a function of volume $V \sim L_\perp$ with $V_1 = 16\,384 r_0^3$. In all four systems, the bilayer membrane contains 1480 lipid molecules and has the projected lipid area $a_{pr} = 1.2 r_0^2$.

volume v_{mol} of the lipids. As discussed in the next section, the measured values of v_{mol} vary within the range of $2.35 < v_{mol}/r_0^3 \leqslant 2.55$ for the systems considered here with $\rho = 3/r_0^3$. This implies that the prefactor $11 - \rho v_{mol} = 11 - 3v_{mol}/r_0^3 > 3$ in Eq. (6) and that the water density ρ_W approaches its asymptotic value $\rho = 3/r_0^3$ from below.

In Fig. 5, the perpendicular water pressure $P_\perp$ is shown as a function of the system volume for four membrane patches all having the same projected lipid area $a_{pr} = 1.2 r_0^2$. The calculation of $P_\perp$ is similar to the calculation of the stress profile described in Ref. 12. For $P_\perp$, we only need to consider the stress tensor component T_{ZZ}. We see that the pressure $P_\perp$ increases with the system volume V and approaches the value of bulk water for large V. In fact, the volume dependence of the water pressure as shown in Fig. 5 is qualitatively similar to the volume dependence of the water density as described by Eq. (6).

In Fig. 6(a), we plot the membrane thickness l_{me} as a function of the inverse lipid area $1/a_{pr}$ for four systems with volumes V_1, V_2, V_3, and V_4. Because of the increased perpendicular pressure, the bilayer thickness decreases with increasing volume $V \sim L_\perp$, which also tends to increase the membrane tension in Fig. 4(c).

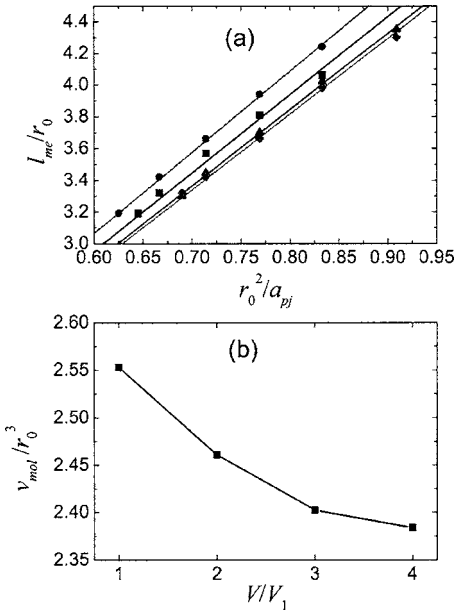

FIG. 6. (a) Membrane thickness l_{me} as a function of the inverse lipid area $1/a_{pr}$ in four simulation boxes with volume $V_1 = 16\,384 r_0^3$ (circles), $V_2 = 2V_1$ (squares), $V_3 = 4V_1$ (triangles), and $V_4 = 8V_1$ (diamonds). Full lines are linear fits. (b) Molecular volume $v_{mol} = \frac{1}{2} l_{me} a_{pr}$ of lipids in the bilayer phase obtained from the linear fits vs the system size $V \sim L_\perp$ for fixed $L_\parallel$.

Transverse finite size effects are not observed for the old parameters used in Ref. 21 where the bead-bead parameters a_{CC}, a_{HH}, and a_{WW} have the same values, see Fig. 4(d). Thus for the old parameter set, lipids are just water beads connected into chains via bond interactions, and the system is more like a one-component rather than a multicomponent system. In this case, thicker water layers do not induce pressure differences inside and outside the bilayer.

Our DPD simulations have been performed in the *NVT* ensemble. To reduce the transverse finite size effects just discussed, one should use the constant pressure ensemble.[30,32,33]

C. Bilayer volume compressibility

In the two previous sections, we have studied the lateral stretching and the transverse thinning of the DPD bilayers. Both types of deformations occur for real lipid bilayers as well. However, real bilayers have a rather large volume compressibility modulus $K_V \simeq 10^{10}$ mJ/m (Ref. 34) which implies that the bilayer volume remains essentially constant during these deformations. Since the repulsive interactions between the DPD beads are provided by soft core potentials, one might expect that the DPD bilayers exhibit a relatively small volume compressibility modulus. However, we will now show that the DPD bilayers have a volume compressibility modulus that is of the same order of magnitude as the one for real bilayers.

In order to study the volume compressibility of the DPD bilayers, we have measured the membrane thickness l_{me} as a function of the projected molecular area a_{pr}. The latter area was varied for fixed total volume V of the simulation box and fixed number of lipids (and water beads) by changing the lateral size $L_\parallel^2$ of the bilayer. In this way, we have obtained four data sets for four different volumes as shown in Fig. 6(a). Inspection of this figure shows that the membrane thickness l_{me} exhibits a linear dependence on the inverse projected area $1/a_{pr}$ for all four values of the total volume V. This linear dependence implies that the molecular volume v_{mol} of the lipid molecule is essentially constant as we stretch the bilayer laterally. Indeed, the molecular volume satisfies the relation $v_{mol} = (1/2) l_{me} a_{pr}$ and is, thus, proportional to the slope of the membrane thickness as a function of $1/a_{pr}$.

For different values of the total volume V, we obtain slightly different values for the molecular volume v_{mol} as shown in Fig. 6(b). The overall change is small, however: as we increase the total volume from $V = V_1$ to $V = V_4 = 8V_1$, the molecular volume decreases from $v_{mol} = 2.55 r_0^3$ to $v_{mol} = 2.38 r_0^3$.

Different values of the total volume V correspond to different perpendicular pressures $P_\perp$ as discussed in the previous section, see Fig. 5. This figure implies that the volume compressibility modulus of the bilayer, which is defined by

$K_V \equiv V(dP/dV)_T$, is of the order of $k_B T/r_0^3$. For room temperature and $r_0 = 0.76$ nm as obtained before by comparison with the projected molecular area of a DMPC bilayer, we then find $K_V \simeq 9 \times 10^9$ mJ/m^3 for the DPD bilayer.

VI. DISCUSSION AND CONCLUSION

The new parameterization for DPD simulation of lipid bilayers introduced in this article gives rise to well-ordered and less stretchable bilayer membranes than previous models. Our basic idea is to reduce the repulsive forces between pairs of interchain tail beads, making them smaller than the force between pairs of water beads. Thus we reduced the corresponding force parameter a_{CC} from $a_{CC}=25$ to $a_{CC}=10$. A further reduction of a_{CC} below $a_{CC}=10$ is not useful since (i) it leads to a shift in the curve $\Sigma = \Sigma(a_{\mathrm{pr}})$ but does not further reduce the stretchability of the bilayer and (ii) it would imply some artificial bead diffusion as discussed by Groot and his co-workers.[19,31] Indeed, these latter authors found that for weak bead-bead repulsion a the diffusion constant attains a constant value for $a<10$. The diffusion constant in such systems is mainly determined by the thermostat rather than by the conservative repulsive forces. Other thermostats, such as the Nosé-Hoover-Lowe-Anderson (NHLAT) thermostat have been introduced to solve this problem.[31] For the latter thermostat, the diffusion constant is found to diverge as a goes to zero. We expect that the NHLAT thermostat combined with DPD repulsive forces may also be useful if we want to reduce the stretchability even further. On the other hand, a "hard core" interaction combined with the DPD thermostat would be an alternative to obtain even less stretchable bilayers.

Usually, oil has a lower density than water. But in Fig. 2, we see that the density of the lipid tails exceeds the density of water. This is caused by the simplifying assumption of the DPD technique that the same amount of matter (in unit of water mass) is contained in each DPD bead for all species. Thus, with reduced repulsive forces between the tail beads, the hydrophobic core becomes more condensed than water. For the simulations of polymersomes, Ortiz *et al.*[23] have used a refined parameter mapping such that the bulk density of the pure species matches experimental data. The new density mapping could also be used in order to further improve the representation of lipid bilayers.

The new parameter set for the DPD simulation of lipid bilayers introduced here may also be used to study tension-induced fusion of membranes. We have already performed preliminary simulations for the fusion of two vesicles which extend previous studies on tension-induced fusion between a vesicle and a planar membrane patch in Ref. 25. Our simulations indicate that fusion occurs via hemifusion for relatively low tensions and via intermediate stalk states for relatively high tensions. These fusion pathways and the associated fusion statistics will be described in more detail in a forthcoming article.

ACKNOWLEDGMENT

The authors thank Andrea Grafmüller for stimulating discussions.

[1] B. Alberts, A. Johnson, J. Lewis, M. Raff, K. Roberts, and P. Walter, *Molecular Biology of Cell*, 4th ed. (Garland Science, New York, 2002).
[2] *Structure and Dynamics of Membranes*, Handbook of Biological Physics, edited by R. Lipowsky and E. Sckmann (Elsevier, Amsterdam, 1995).
[3] W. Rawicz, K. C. Olbrich, T. McIntosh, D. Needham, and E. Evans, Biophys. J. **79**, 328 (2000).
[4] P. Broca, L. Cantu, M. Corti, and E. Del Favero, Prog. Colloid Polym. Sci. **115**, 181 (2000).
[5] D. Needham and R. M. Hochmuth, Biophys. J. **55**, 1001 (1989).
[6] T. Baumgart, S. T. Hess, and W. W. Webb, Nature (London) **425**, 821 (2003).
[7] R. Jahn and H. Grubmüller, Curr. Opin. Cell Biol. **14**, 488 (2002).
[8] D. Harries and A. Ben-Shaul, J. Chem. Phys. **106**, 1609 (1997).
[9] X.-J. Li and M. Schick, Biophys. J. **78**, 34 (2000).
[10] R. G. Larson, J. Chem. Phys. **91**, 2479 (1989).
[11] S. J. Marrink, E. Lindahl, O. Edholm, and A. E. Mark, J. Am. Chem. Soc. **123**, 8638 (2001).
[12] R. Goetz and R. Lipowsky, J. Chem. Phys. **108**, 7397 (1998).
[13] R. Goetz, G. Gommper, and R. Lipowsky, Phys. Rev. Lett. **82**, 221 (1999).
[14] S. J. Marrink, A. H. de Vries, and A. E. Mark, J. Phys. Chem. B **108**, 750 (2004).
[15] M. J. Stevens, J. H. Hoh, and T. B. Woolf, Phys. Rev. Lett. **91**, 188102 (2003).
[16] S. J. Marrink and A. E. Mark, J. Am. Chem. Soc. **125**, 11144 (2003).
[17] P. J. Hoogerbrugge and J. M. V. A. Koelman, Europhys. Lett. **19**, 155 (1992).
[18] P. Espanol and P. Warren, Europhys. Lett. **30**, 191 (1995).
[19] R. D. Groot and P. B. Warren, J. Chem. Phys. **107**, 4423 (1997).
[20] R. D. Groot and K. L. Rabone, Biophys. J. **81**, 725 (2001).
[21] J. C. Shillcock and R. Lipowsky, J. Chem. Phys. **117**, 5048 (2002).
[22] S. Yamamoto, Y. Maruyama, and S. Hyodo, J. Chem. Phys. **116**, 5842 (2002).
[23] V. Ortiz, S. O. Nielsen, D. E. Discher, M. L. Klein, R. Lipowsky, and J. Shillcock, J. Phys. Chem. B **109**, 17708 (2005).
[24] M. Kranenburg, J. Nicolas, and B. Smit, Phys. Chem. Chem. Phys. **6**, 4142 (2004).
[25] J. C. Shillcock and R. Lipowsky, Nat. Mater. **4**, 225 (2005).
[26] E. A. Evans, R. Waugh, and L. Melnick, Biophys. J. **16**, 585 (1976).
[27] R. Kwok and E. Evans, Biophys. J. **35**, 637 (1981).
[28] T. Soddemann, B. Dünweg, and K. Kremer, Phys. Rev. E **68**, 046702 (2003).
[29] E. Evans, V. Heinrich, F. Ludwig, and W. Rawicz, Biophys. J. **85**, 2342 (2003).
[30] T. V. Tolpekina, W. K. den Otter, and W. J. Briels, J. Chem. Phys. **121**, 8014 (2004).
[31] S. D. Stoyanov and R. D. Groot, J. Chem. Phys. **122**, 114112 (2005).
[32] A. E. Jakobsen, J. Chem. Phys. **122**, 124901 (2005).
[33] M. E. Velazquez, A. Gama-Goicochea, M. Gonzalez-Melchor, M. Neria, and J. Alejandre, J. Chem. Phys. **124**, 084104 (2006).
[34] D. March, *Biomembranes: Physical Aspects*, edited by M. Shinitzky (VCH, New York, 1993).